COMPARATIVE ANALYSES OF THE CSSS CALCULATION IN THE UCSD TOMOGRAPHIC SOLAR OBSERVATIONS

T. DUNN[1], B. V. JACKSON[1], P. P. HICK[1], A. BUFFINGTON[1] and X. P. ZHAO[2]

[1]*Center for Astrophysics and Space Sciences, University of California at San Diego, La Jolla, CA, U.S.A.*
[2]*W.W. Hansen Experimental Physics Laboratory, Stanford University, Stanford, CA, U.S.A.*
(e-mail: tdunn@ucsd.edu)

Abstract. We describe a new method to derive the interplanetary magnetic field (IMF) out to 1 AU from photospheric magnetic field measurements. The method uses photospheric magnetograms to calculate a source surface magnetic field at $15R_\odot$. Specifically, we use Wilcox Solar Observatory (WSO) magnetograms as input for the Stanford Current-Sheet Source-Surface (CSSS) model. Beyond the source surface the magnetic field is convected along velocity flow lines derived by a tomographic technique developed at UCSD and applied to interplanetary scintillation (IPS) observations. We compare the results with *in situ* data smoothed by an 18-h running mean. Radial and tangential magnetic field amplitudes fit well for the 20 Carrington rotations studied, which are largely from the active phase of the solar cycle. We show exemplary results for Carrington rotation 1965, which includes the Bastille Day event.

1. Introduction

An important goal of current heliospheric physics is to reconstruct the coronal and heliospheric magnetic field using extrapolations from photospheric magnetic field observations. This endeavor is important for accurate prediction of geomagnetic storms, which are often produced when the southward solar magnetic field arrives at Earth and couples with the Earth's magnetic field (Kamide *et al.*, 1997). The Stanford potential magnetic field model (Hoeksema, Wilcox, and Sherrer, 1983), its Current-Sheet Source-Surface (CSSS) extension (Zhao and Hoeksema, 1995), and similar approaches by others, successfully extrapolate slow changes in the solar surface magnetic field (on the order of a week or more) into the heliosphere. Whether short-term changes (a week or less) in the photospheric magnetic field can be similarly extrapolated to reproduce rapid changes in the interplanetary magnetic field (IMF) at Earth is of significant interest (Jackson, 2002).

There is evidence that photospheric magnetic fields change during coronal mass ejections (CMEs) (Wang *et al.*, 2002) and that these changes may be evident in potential field model reconstructions of the IMF (Luhmann *et al.*, 1998). By incorporating short-term photospheric field changes in the method described in this paper and extrapolating out to Earth, we study whether or not it is possible to anticipate the arrival of CMEs in this manner.

The method we use extrapolates photospheric measurements to produce the interplanetary magnetic field, and compares the results with *in situ* spacecraft observations. Synoptic maps, updated daily or monthly from compilations of photospheric magnetograms, are used to calculate a source surface magnetic field at $15R_\odot$. Specifically, we use Wilcox Solar Observatory (WSO) magnetograms as input for the Stanford Current-Sheet Source-Surface (CSSS) model. Beyond the source surface the magnetic field is convected along velocity flow lines derived by a tomographic technique developed at UCSD (Jackson, Buffington, and Hick, 2001; Jackson, Hick, and Buffington, 2002) and applied to interplanetary scintillation (IPS) observations. IPS data used in this paper are from STELab, Japan (Kojima and Kakinuma, 1987). The global heliospheric results are calculated for month-long intervals on a 1 GHz personal computer in about half an hour. When IPS observations are available in real-time, conditions at 1 AU can be forecast several days in advance.

The next section describes the CSSS model. The third section explains how the CSSS model is combined with the UCSD tomography. The fourth section compares modeled magnetic field amplitude and direction with *in situ* magnetic field observations at Earth for 20 selected time intervals during the most recent solar activity cycle (cycle 23). We show specific results for Carrington rotation 1965, which includes the Bastille Day event, a CME that took place in July of 2000. The fifth section discusses results. We conclude in Section 6.

2. The CSSS Model

The CSSS model chiefly differs from the potential field model by the way it uses two spherical surfaces to divide the solar corona into three separate regions, each with unique physical assumptions. The underlying assumption of the CSSS model is that the interaction between solar wind plasma and the magnetic field can be more realistically recreated using three separate regions, instead of one.

A depiction of the CSSS model is given in Figure 1. The inner region is between the photosphere and the first spherical surface. This first or "cusp" surface, that divides the inner and middle regions, is located near the observed coronal cusp points. The middle region is between the cusp surface and the second spherical surface. This second or "source" surface, that divides the middle and outer regions, is located near the Alfvén critical point. The outer region is the rest of the heliosphere, outside the source surface. The magnetic field calculation in the outer region is based entirely on convection, which is accomplished in this paper using UCSD tomography. The precise placement of the spherical surfaces was experimentally tuned to fit observation (Zhao and Hoeksema, 1995; Zhao, Hoeksema and Rich, 2002). Specifically, the cusp surface is set at $2.25R_\odot$, and the source surface is set at $15R_\odot$.
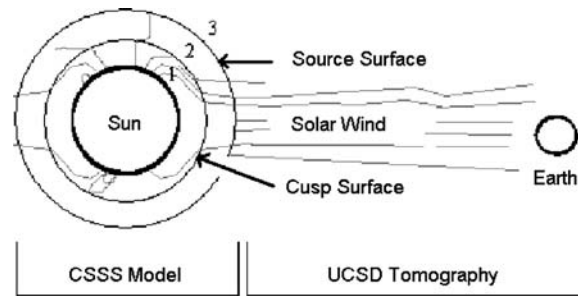
Figure 1. In the inner region (1), the CSSS model calculates the magnetic field using photospheric measurements and a horizontal current model. In the middle region (2), the CSSS model opens the field lines. In the outer region (3), UCSD tomography convects the magnetic field along velocity flow lines (Dunn *et al*., 2002, 2003).

In each region of the CSSS model, different approximations are made to capture the prevailing physics. In the inner region, below the cusp surface, the magnetic field is computed using the global distribution of the observed photospheric magnetic field as a lower boundary condition and applying the "horizontal current model" (Bogdan and Low, 1986) to extrapolate to the cusp surface. The horizontal current model is a solution of magnetostatic equilibrium given the photospheric boundary condition, where electric currents are assumed to be perpendicular to gravity everywhere. The introduction of currents perpendicular to gravity serves to eliminate the gravity term in the equilibrium equation (see Low's derivation in papers published in 1990, 1991). In this way, physically, the CSSS model mimics the interaction between the coronal magnetic field and the solar wind plasma in the inner region by modeling the effect of horizontal currents flowing below the cusp points of helmet streamers. (Alternative methods of modeling hydrostatic equilibria, such as by Neukirch (1995) and Rundenko (2001) are of interest but have not been yet been incorporated into our calculations.)

The cusp surface, between the inner and middle regions, is introduced to allow discontinuous physical conditions. In the inner region, there are no restrictions on the field lines, but the middle region, the field lines must all be open. In the middle region, the CSSS model uses Schatten's method to mimic the effect of the heliospheric current sheet flowing above the cusp points. The effect of the heliospheric current sheet is estimated using the field-reversal technique at the cusp surface (Schatten, 1971). The effect of volume currents beyond Alfvén critical points is obtained using the source-surface technique (Schatten, Wilcox, and Ness, 1969) where field lines are assumed to be radial. With the field-reversal and source-surface technique, field lines are forced to open up. Indeed, observations show that the coronal field becomes open above the cusp-point of helmet streamers. However, the bright streamers are not necessary radial, suggesting that the open field lines may be not radially pointed in general.

At the source surface, all field lines are now assumed to be radial. In the outer region, beyond the source surface, the Archimedean spiral approximation, also known as the "Parker spiral" (Parker, 1958), is used to map the magnetic field from the source surface out to the Earth.

By assuming a constant solar wind speed of $350\,\mathrm{km\,s^{-1}}$ the radial field calculated at the source surface by the CSSS model has been convected from the source surface to 1 AU, and the resulting radial field at 1 AU has been compared with the monthly averaged radial component of the IMF observed at the Earth's orbit (Zhao and Hoeksema, 1995). To lift this restriction of constant solar wind speed, we convect the calculated radial field using the solar wind speed obtained on the basis of the UCSD model and IPS observations.

3. Including the CSSS Model into UCSD Tomographic Reconstructions

In this paper, we convect the magnetic field outwards from the $15R_\odot$ source surface using velocities derived by the UCSD tomography program (Jackson *et al.*, 1998; Jackson, Hick and Buffington, 2002; Hick and Jackson, 2003). The UCSD tomography reconstructs three-dimensional, time-dependent velocity and density matrices by applying an inversion technique to IPS data. In the solar corona, where structures do not evolve significantly (except for corotation) on a time scale of one solar rotation, rotation alone yields sufficient information for reconstruction of the quiet corona (Hurlburt, Martens, and Slater, 1994; Zidowitz, Inhester, and Epple, 1995; Panasyuk, 1999; Frazin, 2000; Frazin and Jansen, 2002) and corotating solar wind.

When a transient structure such as a heliospheric response to a CME is observed across a large range of solar elongations (as in the IPS observations), it is seen from widely different directions as it moves past Earth. This changing perspective is used by the UCSD tomography to construct (or "invert") a three-dimensional solar wind model. The UCSD technique takes into account the fact that line-of-sight IPS observations are dominated by contributions from material closest to the Sun, because more scattering occurs there, but makes no explicit assumptions about the distribution of velocity and density along these lines of sight.

The tomographic inversion process begins by creating a set (in time) of initial boundary conditions for each source surface at regular time cadence throughout the interval of the three-dimensional reconstruction. These lower boundaries (the source surfaces) are populated with an unstructured approximation of mass and velocity at $15R_\odot$. Currently, the UCSD model propagates mass and velocities outward from the source surface to beyond Earth using a purely kinematic model. The model assumes radial outflow and enforces conservation of mass and mass flux (Jackson *et al.*, 1998). Thus, given the initial velocities and densities on the inner boundaries, a fully three-dimensional solar wind model over time is created in the inner heliosphere. This three-dimensional time-dependent result is then compared with

line-of-sight IPS scintillation levels and IPS fluctuation levels perpendicular to the line-of-sight observations. (In order for corresponding measurements to be compared, line-of-sight values are generated from the solar wind reconstruction results, that correspond to the type of observational data used.) The differences between the two data sets are used to update the initial mass and velocity distribution on the source-surface boundaries of the three-dimensional reconstruction. A least-squares best fit is derived iteratively: if the inner boundary values do not produce a solar wind at large solar distances that reproduce the observations accurately enough, the source-surface values of density and velocity are iteratively updated based on the differences between the reconstruction and the IPS observations. Convergence is assumed when differences no longer change by more than a few percent, and this is normally well within 18 iterations of the updating procedure.

Only a few thousand lines of sight exist in any given solar rotation, and so the spatial and temporal resolution that is maintained by a set of Gaussian filters is at best only about $20° \times 20°$ in latitude and longitude, having a 1-day temporal cadence. Nevertheless, the resolution is sufficient to determine the large-scale features of CME velocity and density structure. Tests show that after a few iterations any information from the initial distribution used to begin the iterative process is lost. The technique has been successfully used to analyze CME-associated velocity and density structures using both IPS and Thomson scattering observations (Jackson and Hick, 2004) and these compare favorably with other techniques used to invert the IPS data (Tokumaru *et al.*, 2003).

These velocities from the three-dimensional UCSD reconstruction are then used to calculate the magnetic field. Since the plasma has high electrical conductivity, we assume that outside the source surface, the magnetic field is frozen into the plasma (Hundhausen, 1972), and follows the flow lines of the velocity. Assuming a solar wind with constant outflow velocity V, the magnetic field components are:

$$B_r(r, \phi, \theta) = B(r_0, \phi_0, \theta_0)\left(\frac{r_0}{r}\right)^2,$$ (1)

$$B_\phi(r, \phi, \theta) = -B(r)\left(\frac{\omega r_0 \sin(\theta)}{V}\right)\left(\frac{r_0}{r}\right),$$ (2)

$$B_\theta(r, \phi, \theta) = 0.$$ (3)

Here r, ϕ, and θ are the usual spherical coordinates, and $B(r_0, \phi_0, \theta_0)$ is the magnitude of the magnetic field at the $15R_\odot$ source surface of the CSSS model, where it is presumed to be purely radial. The solar angular rotation is ω rad s^{-1}. Since we are not restricted to a constant velocity, we choose $V = V(r, \phi, \theta)$ from the tomography as the relevant outflow velocity at location (r, ϕ, θ) in the heliosphere, in accordance with Gauss's law. Since the magnetic field is assumed radial at the source surface, B_ϕ is introduced by solar rotation at large distances from the source surface. $B(r_0, \phi_0, \theta_0)$ varies in time.

The final result is a three-dimensional magnetic field model extending from $15R_\odot$ to beyond Earth. The current time-dependent UCSD tomography has a resolution of about 0.25 AU in heliocentric distance and $20° \times 20°$ in heliographic longitude and latitude, with a time cadence of 1 day. The next section compares both the radial and tangential components of the magnetic field with *in situ* results at Earth. Since we assume that the magnetic field is entirely radial at the source surface, the magnetic field in the outer region has no theta component.

4. Comparison with Observations

We analyze a sequence of Carrington rotations from CR 1956 to CR 2006. For each rotation, time series for density, velocity and radial and tangential magnetic field components (B_r and B_ϕ, respectively) at Earth are extracted from the three-dimensional model. These are compared with *in situ* ACE data for the same time period by converting data from three-component GSM to RTM coordinates (B_r, B_ϕ, B_θ). Since we can only model radial and tangential magnetic fields using the potential field model extrapolations, these are the only two components compared with the ACE data. In general, the *in situ* B_θ component is nearly as large as the B_ϕ component. Our current model does not take this into account. For control, we also analyze time series results when UCSD tomography is not used. In this case, we assume a constant outflow velocity of 500 km s^{-1} outside the source surface, commensurate with observations at solar maximum (Schwenn, 1990). Constant speeds of 400 and 600 km s^{-1} were also tested and produced a poorer fit.

Figures 2–4 represent time series and correlations of modeled magnetic field with *in situ* ACE data from Carrington rotation 1965, close to the maximum of solar cycle 23. Figure 2a and b show time series and correlations for the radial and tangential magnetic field model using monthly updated maps. Figure 3a and b show time series and correlations for the radial and tangential magnetic field model instead using daily updated maps. Figure 4a and b show time series and correlations for the velocity and density reconstructed from UCSD tomography. In Figure 2a and b, the *in situ* data are smoothed by a 7-day running mean, which best fits the monthly updated magnetic model. In all other plots, the *in situ* data shown are smoothed by an 18-h running mean, which is commensurate with the spacetime resolution of the velocity matrix from the UCSD tomography at Earth's orbit. The dashed lines are linear fits on the model data. The solid lines are linear fits on the observed data.

There is an acceptable correlation between ACE data and our model for Carrington rotation 1965, which includes the Bastille Day CME that reached Earth on 15 July 2000. Using daily updated maps (Figure 3) we obtain correlations of 0.73 and 0.50 in radial and tangential components, respectively. Earlier models, which used monthly updates, achieved significantly higher correlations, as in Figure 2.
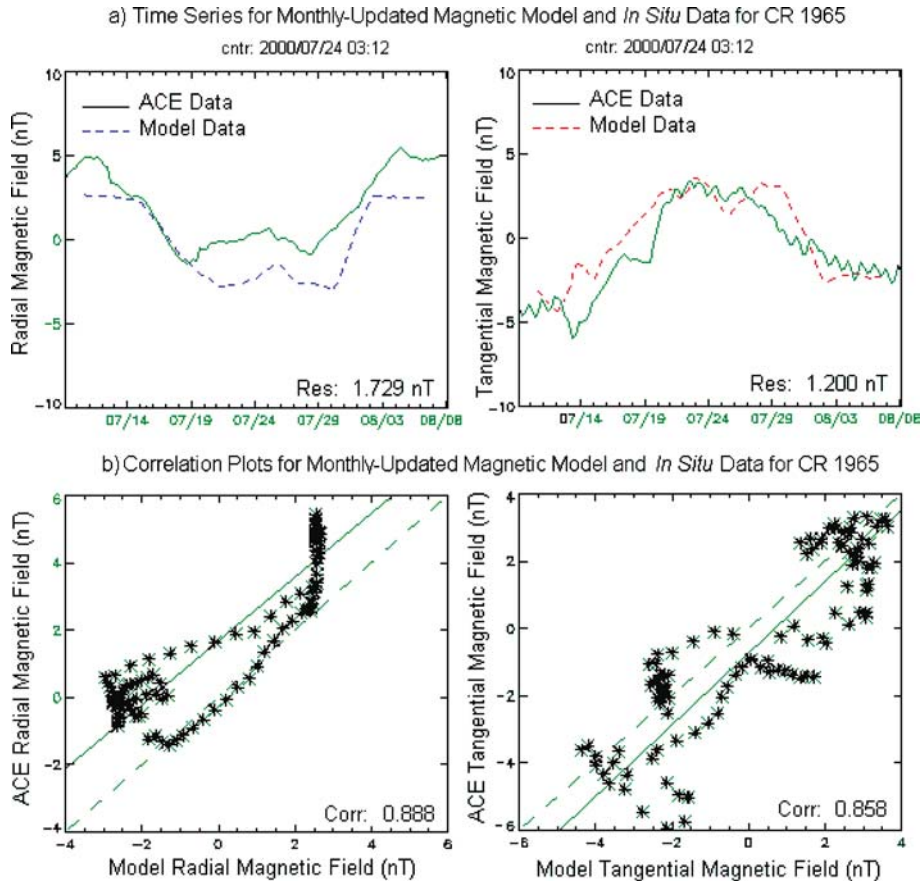
a) Time Series for Monthly-Updated Magnetic Model and *In Situ* Data for CR 1965

b) Correlation Plots for Monthly-Updated Magnetic Model and *In Situ* Data for CR 1965

Figure 2. (a) Time series for the monthly model magnetic field and the 7-day average *in situ* magnetic field. (b) Correlation plots. The 45° *dashed line* in the correlation plots indicates the location of one-to-one correspondence. The shorter *solid line* indicates the linear least-squares fit to the points shown. The radial component of the magnetic field is on the left, and the tangential component is on the right.

In these analyses, 7-day averaged *in situ* data were used and small-scale variations were not as apparent (Dunn *et al.*, 2002, 2003).

Since linear correlation coefficients only give a measure of how well a linear relation fits model to observation, it is useful to calculate the residual between the model and the *in situ* time series for each Carrington rotation. This gives a direct measure of how well the model amplitude fits the *in situ* observations. In this paper, the mean absolute difference, or residual *Res*, is calculated as:

$$Res = \frac{1}{N} \sum |x_i - y_i|. \tag{4}$$

Here N is the number of data points measured in a given Carrington rotation, evenly spaced in time, along Earth's orbit. For each data point x_i from the model there is
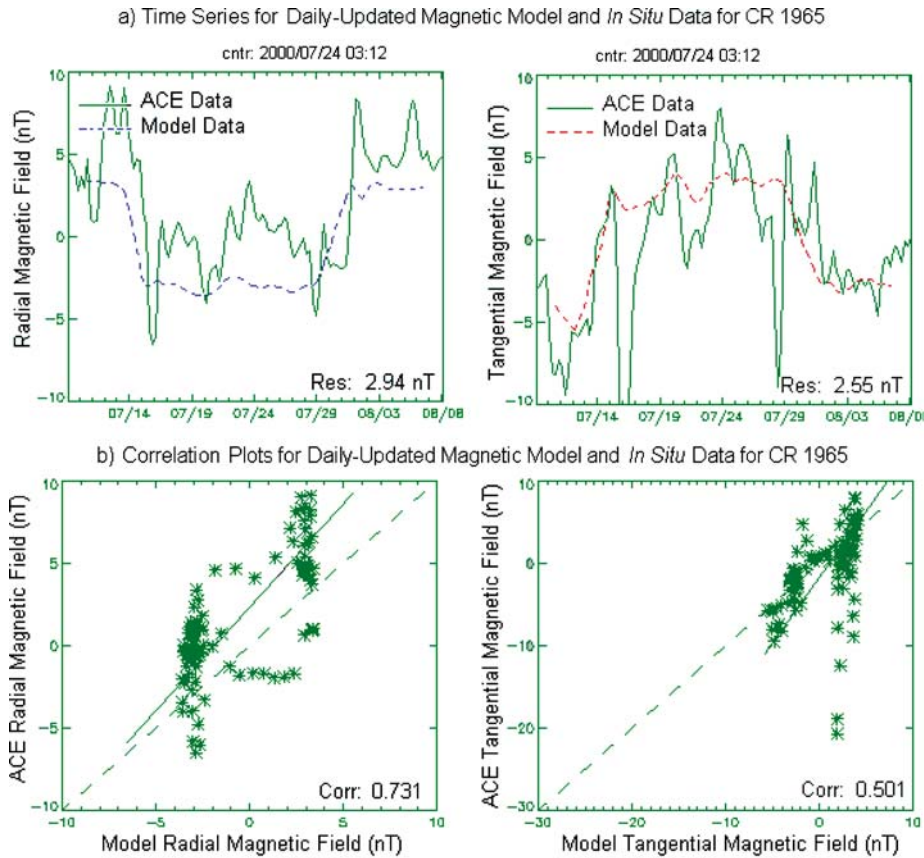
Figure 3. (a) Time series for the daily model magnetic field and the 18-h average *in situ* magnetic field. (b) Correlation plots. The 45° *dashed line* in the correlation plots indicates the location of one-to-one correspondence. The shorter *solid line* indicates the linear least-squares fit to the points shown. The radial component of the magnetic field is on the left, and the tangential component is on the right.

a corresponding point y_i that is extracted from *in situ* data, at the same time and location. For Carrington rotation 1965, residuals are 2.9 and 2.6 nT, in radial and tangential components, respectively, when daily updated maps are used.

Model velocities determine the arrival timing at ACE of the magnetic field components. For B_ϕ they are also used to derive the magnetic field component. Figure 5 shows how the tangential component of the magnetic field (which, as in Equation (2), is dependent on solar wind velocity, while the radial component is not) varies with the model parameters. Again, the time series and correlation comparisons are with *in situ* ACE data for Carrington rotation 1965. Figure 5a shows the time series and correlations for the most simplistic model, where monthly magnetic maps are used as input, and a constant velocity of 500 km s^{-1} is used to convect the field out to 1 AU. Figure 5b shows the time series and correlations

a) Time Series for IPS Velocity (left) and Density (right) and *In Situ* Data for CR 1965

b) Correlation Plots for IPS Velocity (left) and Density (right) and *In Situ* Data for CR 1965
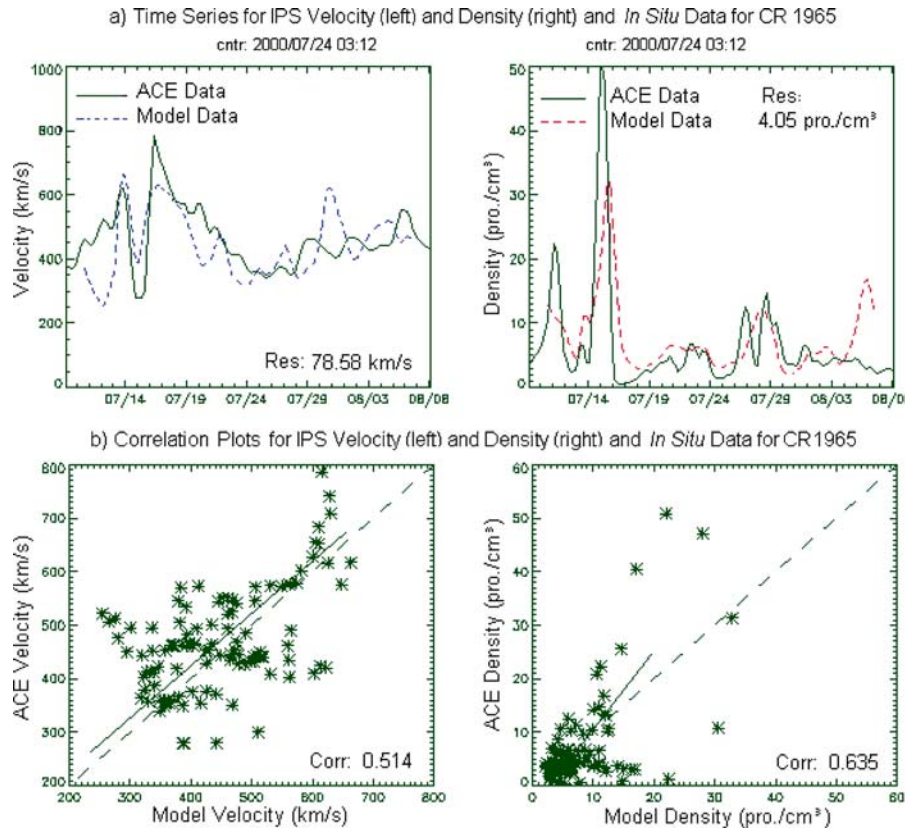
Figure 4. (a) Time series for the reconstructed velocities (*left*) and densities (*right*) with the 18-h average *in situ* data. (b) Correlation plots. The 45° *dashed line* in the correlation plots indicates the location of one-to-one correspondence. The shorter *solid line* indicates the linear least-squares fit to the points shown.

when monthly magnetic maps are used, and the velocities are reconstructed by the UCSD tomography. Figure 5c and the right of Figure 3 show the time series and correlations when daily-updated magnetic maps are used, again using reconstructed velocities. In Figures 3–5, the *in situ* data shown are smoothed by an 18-h running mean.

Figure 5 shows that the large-scale correlation remains approximately the same for all three plots, even though the complexity of the model increases. Meanwhile, the residual slightly decreases. The drop in residual denotes an improvement in the capture of small-scale fluctuations. However, single excursions on the order of 10 nT and almost 1 day in duration are not reproduced.

Figures 2–5 are for only one exemplary rotation. A set of 20 Carrington rotations from years 1999 to 2003, selected for completeness of IPS data, availability of WSO magnetic maps, and availability of ACE data, were similarly analyzed. Over

Time Series for 3 Models and *In Situ* Data for CR 1965
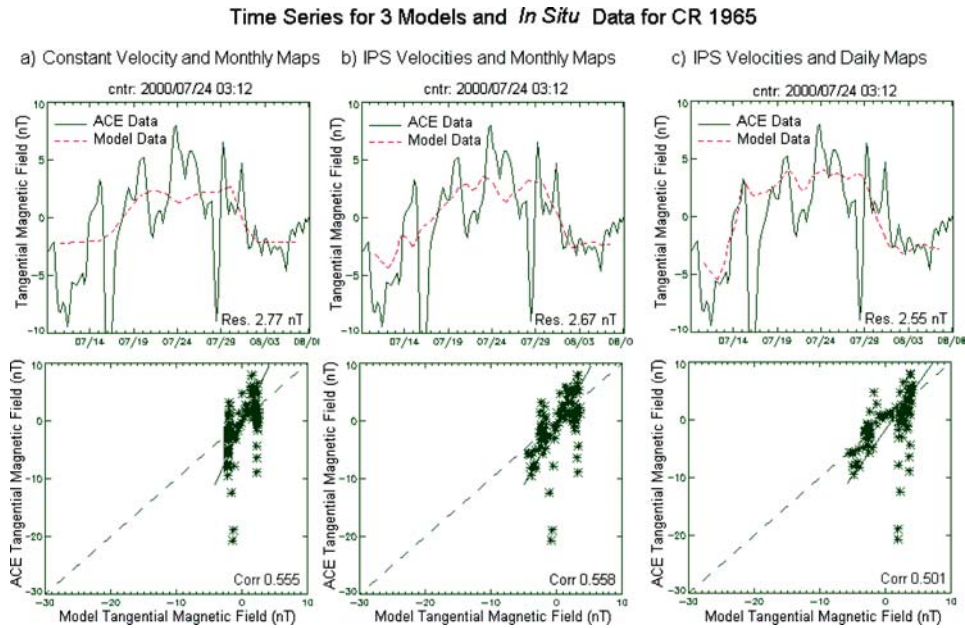
Figure 5. Time series plots and correlation for the model tangential magnetic field and the *in situ* tangential magnetic field. (a) Monthly updated magnetic maps and constant velocity input to the model. (b) Monthly updated magnetic maps and reconstructed velocities input to the model. (c) Daily updated magnetic maps and reconstructed velocities input to the model.

the 20 rotations, models using monthly updated maps and IPS tomography yielded average correlations of 0.64 and 0.56 in radial and tangential magnetic field components, respectively, and average residuals of 2.6 and 2.2 nT, respectively. Models using daily updated maps yielded average correlations of 0.64 and 0.56 in radial and tangential components, respectively, and average residuals of 2.7 and 2.4 nT, respectively.

5. Analysis of Results

Figure 4b shows that there is often a high correlation between model and *in situ* velocity observations, even for short-term variations, and in fact CME structure is fairly well reproduced in both velocity and density in the UCSD time-dependent tomography (Jackson, Hick, and Buffington, 2002). In this section, we look for a relationship between how well velocity is reconstructed by IPS and how well the magnetic field is reconstructed at Earth by our model. We also investigate why not all variation in the *in situ* field is reproduced by the model.

Since the reconstructed velocities convect the magnetic field, we expect that a relationship exists between how well velocity is reconstructed and how well the
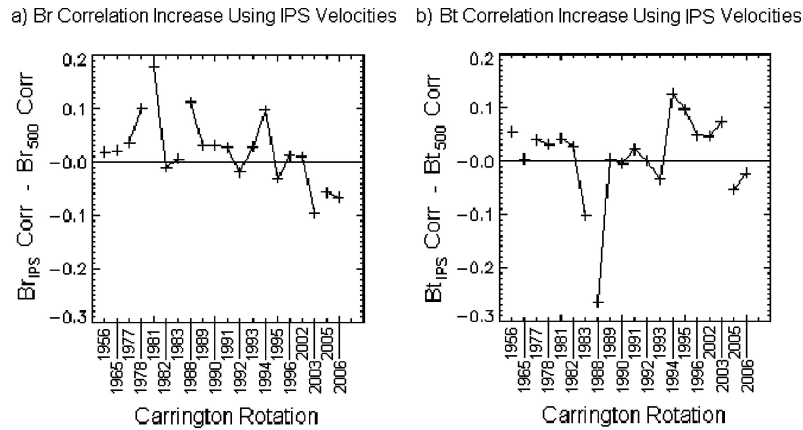
a) Br Correlation Increase Using IPS Velocities   b) Bt Correlation Increase Using IPS Velocities

Figure 6. Correlation differences for 20 Carrington rotations between model using reconstructed velocities and model using a constant velocity: (a) for the radial component of magnetic field; (b) for the tangential component of magnetic field.

magnetic field is reconstructed. For example, Figure 5 shows a clear improvement in the model when IPS is used, and the reconstructed velocities show a good fit for this rotation. To test this systematically, we do two things. First, we compare our model results with the results from using a constant velocity, over 20 rotations. Second, we look for a relationship between velocity correlation/residual and magnetic field correlation/residual, over 20 rotations.

Figure 6 addresses the first test. Each cross in the figure represents the difference in correlation values for the magnetic field using reconstructed velocities and using a constant 500 km s^{-1} velocity, respectively, for 20 Carrington rotations. Thus, a cross at position (x, y) signifies that the correlation using IPS data is y better than the correlation using a constant velocity, for Carrington rotation x. Where the crosses are joined by lines, the Carrington rotations plotted are consecutive and the x-axis is equidistant. A break in the lines between crosses denotes a gap in the sequence of available Carrington rotations, and the x-axis is contracted. We see that the reconstructed velocities give a very slight increase in correlation for the monthly updated magnetic field model over using the constant velocity model. There is no analogous increase for daily updated maps. When we compare the residuals for the monthly- and daily updated models with the residuals from the constant velocity results, there is no clear improvement.

As for the second test, there is no obvious relationship between how well the velocity reconstructions correlate and how well the magnetic field model correlates. There is also no obvious relationship between velocity residuals and magnetic field residuals.

Lastly, we investigate why not all variation in the *in situ* field is reproduced by the model. It is natural to expect that not all velocity variations can be reproduced

by the tomography with a limited number of viewpoints. However, our magnetic model does not reproduce variation in magnetic field with the same resolution as the velocity. Specifically, large variations in the solar wind velocity observed at 1 AU are often reproduced accurately (Figure 5; Jackson, Hick, and Buffington, 2002). Similarly, we expect that temporal and spatial variations in the magnetic field at the source surface are convected outward accurately, and that they produce sufficient variations in time series at 1 AU. Indeed, we do reproduce the large-scale variations in the *in situ* magnetic field (e.g. associated with sector boundary crossings). However, even when using daily updated photospheric synoptic maps, the time series of the model magnetic data show less variation than the 18-h averaged *in situ* data (Figure 4a). Variations on the order of 10 nT (several times the background magnetic field strength) and time scales of 1 day observed at 1 AU are not reproduced accurately in our model.

A peak of 1 day in a time series at 1 AU can be introduced by a persistent spatial peak in the background magnetic field with a width of about 1 grid spacing ($20°$) at the source surface corotating past Earth, or, alternatively, a transient variation in field strength over a 1-day time period that convects past Earth in the solar wind. Within the context of our modeling, we can distinguish three possible origins of the short-term magnetic variations observed *in situ*: 1) variations are introduced in the inner heliosphere outside the source surface, 2) variations are introduced in the corona between photosphere and source surface, or 3) variations (spatial and/or temporal) are already present in the photospheric magnetic field.

If, as in the first possibility, variations are produced outside the source surface, then our ability to detect these variations depends on the capability of the (time-dependent) kinematic solar wind model used in the tomographic reconstructions to reproduce the solar wind interactions that cause the short-term magnetic variations *in situ*. Since we do accurately reproduce large variations in the solar wind velocity observed at 1 AU (Figure 5; Jackson, Hick, and Buffington, 2002), we feel that our current solar wind model, in spite of its rudimentary physics, should be able to reproduce the spatial and temporal magnetic variations to some extent. Thus, we do not feel that the first possibility is a likely explanation.

With respect to the second possibility, if variations are produced in the corona (with no or little impact on the underlying photospheric field) we do not expect to see these variations in our modeling. Since we take photospheric magnetic fields as input and extrapolate outward from there, we are essentially "blind" to this type of variation.

The third, remaining possibility is that variations are produced at the photosphere, which gives rise to a more complicated situation. In the CSSS model, the polynomial expansion of the magnetic field emphasizes large-scale magnetic structures at the source surface. Only the most basic structures are projected to the cusp surface, and so they will dominate the structure of the source surface magnetic field. Thus, the source surface magnetic maps used as input for the tomographic model show little spatial fine structure, and persistent small-scale spatial peaks in

the photosphere do not have a significant small-scale signature at the source surface. Even if not "blind", our modeling is not very sensitive to small-scale photospheric changes. This is to be expected from a steady-state coronal model, such as the CSSS model, or any model that simply extrapolates magnetic flux outward from the solar surface preserving the dominant magnetic components.

In summary, the inability of our model to reproduce short-term (<1 day) variations in the magnetic field at 1 AU may originate from either (or both) of the remaining possibilities, 2 and 3. According to the second possibility, the short-term variations originate in the corona below the source surface, with little impact on the underlying photospheric magnetic field. This condition could occur, for instance, for coronal mass ejections that often involve a major rearrangement of coronal magnetic fields on short time scales without necessarily changing the photospheric magnetic field significantly. According to the third possibility, the short-term variations at 1 AU are already present as temporal variations in the daily updated photospheric maps, but the steady-state model does not allow these to be projected outward accurately to the source surface.

The second possibility could only be addressed by including the coronal magnetic field variation information and a time-dependent model capable of reproducing the short temporal variations of coronal magnetic field associated with transient events. The third possibility could in principle be addressed by using a time-dependent coronal model capable of handling a time-varying background magnetic field with a sequence of daily updated photospheric maps as an imposed boundary condition. This would better model the effects of photospheric temporal variations at the source surface. Both of these projects lie well beyond the scope of the analysis presented here.

6. Conclusion

Tomographic techniques developed at UCSD provide a three-dimensional solar wind model sufficient to determine global velocity and density variation in the inner heliosphere. These velocities, when applied to results of the CSSS model, provide a new method for extrapolating the magnetic field out to Earth, where it can be compared with *in situ* spacecraft measurements. Generally, the magnitude of the magnetic field is acceptably reproduced. The velocity, density, and magnetic field results can be forecast several days in advance using modest computational resources if IPS observations are available in (near-) real time.

On average, the combination of using monthly updated photospheric maps and reconstructed velocities slightly improves the fit to *in situ* data, while daily updated maps do not. This trend is not the case for all rotations studied. The difference may be because, while the daily updates allow us to capture rapid changes of large-extent characteristic of particular Carrington rotations, such as in CR 1965, the updates also introduce more noise.

Single excursions on the order of 10 nT and 1 day in duration at 1 AU are often not reproduced by our method. Daily updated maps and velocities that vary on an 18-h timescale are not sufficient to reproduce these excursions. To track these magnetic excursions with the current kinematic IPS model, a magnetic source surface more time-variable and complex than is currently available is required. We hope that MHD codes and vector magnetograms will reveal the short-term photospheric manifestation of a CME. However, this is not assured, since in our analyses, rapidly updated magnetograms have not revealed the emergence of CMEs. The great concern for our science is that while photospheric information is sufficient to recreate the ambient IMF, it is not sufficient to reliably reveal the ejection of CMEs.

Acknowledgements

References

Bogdan, T. J. and Low, B. C.: 1986, *Astrophys J.* **306**, 271.
Dunn, T., Hick, P. P., Jackson, B. V., and Zhao, X.: 2002, *SPIE Proc.* **4853**, 6.
Dunn, T., Hick, P. P., Jackson, B. V., and Zhao, X.: 2003, *SPIE Proc.* **4853**, 504.
Frazin, R. A.: 2000, *Astrophys. J.* **530**, 1026.
Frazin, R. A. and Janzen, P.: 2002, *Astrophys. J.* **570**, 408.
Hick, P. P. and Jackson, B. V: 2003, *SPIE Proc.* **5171**, 287.
Hoeksema, J. T., Wilcox, J. M., and Sherrer, P. H.: 1983, *J. Geophys. Res.* **88**, 9910.
Hundhausen, A. J.: 1972, *Solar Wind and Coronal Expansion*, Springer-Verlag, New York, p. 10.
Hurlburt, N. E., Martens, P. C. H., and Slater, G. L.: 1994, in Balasubrumanian, K. S., Simon, G. W. (eds.), *Solar Active Region Evolution: Comparing Models With Observations, ASP Conf. Series*, **68**, 30.
Jackson, B. V.: 2002, *BAAS* **34**(2), 751.
Jackson, B. V., and Hick, P.: 2000, *Adv. Space Res.* **29** (3), 1875.
Jackson, B. V. and Hick, P. P., 2004, in D. E., Gary, and Ch. O., Keller (eds.), *Solar and Space Weather Radio Physics*, Kluwer, ASSL, Vol. 314, p. 353.
Jackson, B. V., Buffington, A., and Hick, P. P.: 2001, *Proceedigs of the Solar Encounter: The First Solar Orbiter Workshop*, p. 251.
Jackson, B. V., Hick, P. P., and Buffington, A.: 2002, *Proceedings of Solar Wind*, Vol. 10, p. 75.
Jackson, B. V., Hick, P. P., Kojima, M., and Yokobe, A.: 1998, *J. Geophys. Res.* **103**, 12049.
Kojima, M. and Kakinuma, T.: 1987, *J. Geophys. Res.* **92**, 7269.
Kamide, Y., McPherron, R. L., Gonzalez, W. D., Hamilton, D. C., Hudson, H. S., Joselyn, J. A., Kahler, S. W., Lyons, L. R., Lundstead, H., and Szuszczewicz, E.: 1997, in B. T. Tsurutani, W. D. Gonzalez, Y. Kamide, J. K. Arballo (eds.), *Geophysical Monograph*, American Geophysics Union, AGU, Washington, DC, p. 1.

Luhmann, J. G., Gosling, J. T., Hoeksema, J. T., and Zhao, X.: 1998, *J. Geophys. Res.* **103**, 6585.

Neukirch, T.: 1995, *Astron. Astrophys.* **301**, 628.

Panasyuk, A. V.: 1999, *J. Geophys. Res.* **104**, 9721.

Parker, E. N.: 1958, *Astrophys. J.* **128**, 664.

Rudenko, G. V.: 2001, *Solar Phys.* **198**, 279.

Schwenn, R.: 1990, in R. Schwenn and E. Marsch (eds.), *Physics and Chemistry in Space*, Vol. 1, Springer-Verlag, Berlin, p. 99.

Schatten, K., Wilcox, J. W., and Ness, N. F.: 1969, *Solar Phys.* **6**, 442.

Schatten, K. H.: 1971, *Cosmic Electrodyn.* **2**, 232.

Tokumaru, M., Kojima, M., Fujiki, K., and Yamashita, M.: 2003, in M. Velli, R. Bruno, F. Malara (ed), *Proceedings of the Solar Wind Ten, AIP Conference*, Vol. 679, Melville, New York, p. 729.

Wang, H., Spirock, T., Qiu, J., Ji, H., Yuchyshyn, V., Moon, Y. J., Denker, C., and Goode, P.: 2002, *BAAS* **576** (1), 497.

Zhao, X. P. and Hoeksema, J. T.: 1995, *J. Geophys. Res.* **100** (A1), 19.

Zhao, X. P., Hoeksema, J. T., and Rich, N. B.: 2002, *Adv. Space Res.* **29** (3), 411.

Zidowitz, S., Inhester, B., and Epple, A.: 1995, in D. Winterhalter, J. T. Gosling, S. R. Habbal, W. S. Kurth, and M. Neugebauer (eds.), *Proceedings of the Solar Wind Eight, AIP Conference*, Vol. 382, Woodbury, p. 165.